Journal of Power Sources 189 (2009) 169–178

Contents lists available at ScienceDirect

Journal of Power Sources

journal homepage: www.elsevier.com/locate/jpowsour

Electrochemical properties of $LiFePO_4$ prepared via ball-milling

George Ting-Kuo Fey[a,*], Yun Geng Chen[a], Hsien-Ming Kao[b]

[a] Department of Chemical and Materials Engineering, National Central University, Chung-Li 32054 Taiwan, ROC
[b] Department of Chemistry, National Central University, Chung-Li 32054 Taiwan, ROC

ARTICLE INFO

Article history:
Received 17 June 2008
Received in revised form
30 September 2008
Accepted 1 October 2008
Available online 17 October 2008

Keywords:
$LiFePO_4$
Lithium-ion batteries
Cathode
Particle size
Ball-milling

ABSTRACT

$LiFePO_4$ cathode materials with distinct particle sizes were prepared by a planetary ball-milling method. The effects of particle size on the morphology, thermal stability and electrochemical performance of $LiFePO_4$ cathode materials were investigated. The ball-milling method decreased particle size, thereby reducing the length of diffusion and improving the reversibility of the lithium ion intercalation/deintercalation. It is worth noting that the small particle sample prepared using malonic acid as a carbon source achieved a high capacity of 161 mAh g^{-1} at a 0.1 C rate and had a very flat capacity curve during the early 50 cycles. However, the big particle samples (~400 nm) decayed more dramatically in capacity than the small particle size samples (~200 nm) at high current densities. The improvement in electrode performance was mainly due to the fine particles, the small size distribution, and the increase in electronic conductivity as a result of carbon coating. The structure and morphology of the ground $LiFePO_4$ samples were characterized with XRD, FE-SEM, TEM, EDS, and DSC techniques.

1. Introduction

Olivine $LiFePO_4$ has received widespread attention as a promising cathode material for high power applications, such as power tools or hybrid electric vehicles, following Padhi's publication [1]. This low cost material also has the advantages of low toxicity [2], high thermal stability [3], high capacity (170 mAh g^{-1}) [4], good cycling stability, and a flat discharge plateau (at 3.4 V) [5]. Although it has many advantages, it has problems with very low conductivity about 10^{-9} S cm^{-1} and slow Li ion diffusion across the $LiFePO_4$/$FePO_4$ two-phase boundary during the charge–discharge process [6,7]. The low ionic and electronic conductivity results in low discharge capacity, high polarization and poor rate capability.

To overcome these problems, the strategies of preparing particles with a small size [8,9] coating electronically conductive carbon on the surface of $LiFePO_4$ [10–13] and using supervalent cation doping in the lattice of $LiFePO_4$ [14] have been proposed by many research groups.

The carbon coating method provides pathways for electron transference, which improve lattice electronic conductivity and lithium-ion diffusion within a crystal [15]. The lowest amount of carbon in $LiFePO_4$/C should allow enough diffusion to overcome the conductivity limitations of $LiFePO_4$. In addition, many researchers have found that substituting Li^+ or Fe^{2+} with supervalent cations to create p-type semiconductors can enhance the bulk conductivity of $LiFePO_4$ [15–17]. The above-mentioned methods greatly influenced both electronic and ionic conductivities of materials in terms of capacity delivery, cycle life and rate capability.

Other possible methods for improving the rate performance of $LiFePO_4$ materials are to enhance ionic/electronic conductivity by optimizing particles with suitable preparation procedures. Moreover, some literature indicates that lithium ion diffusion capability can become a key factor that affects the rate capacity of $LiFePO_4$ [18]. In order to synthesize fine and homogenous nanoparticles of $LiFePO_4$, several techniques have been applied to prepare $LiFePO_4$ under different conditions, including the sol–gel method [19], co-precipitation in an aqueous medium [20], a hydrothermal procedure [21], and mechanochemical activation [22].

Nowadays, ball-milling synthesis is a useful method for preparing fine particles. It is also simple and energy efficient. Xia et al. [23] have already demonstrated the ball-milling synthesis of $LiFePO_4$.

In our work, we used ball-milling to grind commercial (commercial product of Aleees) and in-house $LiFePO_4$ powders for comparison and evaluation. Furthermore, we tried to investigate the effects of particle size on the surface area, morphology, polarization, electronic conductivity, thermal stability and cell performance of the $LiFePO_4$ materials.

2. Experimental

2.1. Synthesis of in-house bare-$LiFePO_4$

The in-house bare-$LiFePO_4$ powders were prepared using lithium carbonate (Merck, 99%), iron(II) oxalate dehydrate(Showa,

* Corresponding author. Tel.: +886 3 425 7325; fax: +886 3 425 7325.
E-mail address: gfey@cc.ncu.edu.tw (G.T.-K. Fey).

0378-7753/$ – see front matter © 2008 Elsevier B.V. All rights reserved.
doi:10.1016/j.jpowsour.2008.10.016

98%), and ammonium dihydrogen phosphate(Sigma, 99%) in a stoichiometric molar ratio (1.03:1:1) by a high temperature solid-state method, details of which are given elsewhere [24].

2.2. Preparation of distinct particle size samples

To lower preparation cost, we selected a planetary ball-mill that produced distinct particle size powders under different milling times. The commercial and in-house bare-$LiFePO_4$ powders denoted as Com-LFP and Lab-LFP, respectively, were ground in a planetary ball-mill with a rotation speed of 300 rpm for 3 h in acetone under an air atmosphere. Mass ratio of the materials to zirconia balls (diameter: 0.1 mm) was selected to be 1:20. The ground powders were dried and reground with a rotation speed of 300 rpm for 3 h again in acetone under an air atmosphere at room temperature. The above process was repeated 1, 4 and 6 times. The distinct particle size powders of Com-LFP and Lab-LFP powders after 1, 4 and 6 times or 3 h, 12 h, and 18 h of grinding were obtained in three different particle sizes: 418, 292, 202 nm and 462, 315, 188 nm, respectively. The standard deviation of particle size was ±10.

2.3. The ground powders treated with carbon coating

The ground Com-LFP powders obtained after drying could be considered as uncoated particles because the mechanical impact might damage the already formed carbon coating layer. These powders were further treated using malonic acid (Fluka, 98%) as the carbon source by a rheological phase reaction using evaporation.

The carbon precursor was prepared by ball-milling the mixture of $LiFePO_4$ powders and 50 wt.% malonic acid for 1 h and pressing it into a pellet, which was heated at 873 K for 12 h in an Ar/H_2 (vol. 95:5) atmosphere. The ground powder sample to be coated was placed downstream from the carbon-precursor pellet in a tube furnace. The ground powders and carbon pellet were 2 cm apart and the diameter of the carbon pellet was 1.2 cm. The carbon-coated $LiFePO_4$ powders for the commercial and in-house bare samples are denoted as Com-LFP/C and Lab-LFP/C, respectively.

2.4. Characterization

Structural analysis was carried out using a powder X-ray diffractometer (XRD), Siemens D-5000, Mac Science MXP18, equipped with a nickel-filtered Cu K$_\alpha$ radiation source (λ = 1.5405 Å). The diffraction patterns were recorded between scattering angles of 15° and 80° in steps of 0.05°. The morphology of the $LiFePO_4$/C composite was observed with a scanning electron microscope (SEM; Hitachi S-3500 V) and high-resolution transmission electron microscope (HR-TEM; Jeol TEM-2000FXII). The particle size distribution was also measured by a dynamic light-scattering particle size analyzer (Malvern Zetasizer Nano). The Brunauer, Emmett, and Teller (BET) method was used to measure the surface area of the powders (ASAP 2010 Analyzer). Conductivity was measured by four-point conductivity measurements with a Keithley Model 2400S source meter.

2.5. Electrochemical characterization

Coin cells of the 2032 configuration were assembled in an argon-filled VAC MO40-1 glove box in which the oxygen and water contents were maintained below 2 ppm. The cathode was prepared by mixing 85 wt.% carbon-coated $LiFePO_4$ powder with 10 wt.% conductive carbon black and 5 wt.% polyvinylidene fluoride (PVDF) in a *n*-methyl-2-pyrrolidone (NMP) solution, which was then applied onto an etched aluminum foil current collector and dried at 393 K for 12 h in an oven. Lithium metal (Foote Mineral) was used as the anode and a 1 M solution of $LiPF_6$ in EC:DEC (1:1, v/v) (Tomiyama Chemicals) was used as the electrolyte with a Celgard membrane as the separator.

The cells were cycled at a 0.2 C rate between 2.8 and 4.3 V in a multi-channel battery tester (Maccor 4000). Phase transitions during the cycling processes were examined by slow-scan cyclic voltammetric studies, where the cells were assembled inside a glove box with lithium metal foil serving as both counter and reference electrodes. The electrolyte used was the same as that for the coin cell. Cyclic voltammograms were run on a Solartron 1287 Electrochemical Interface at a scan rate of 0.1 mV s^{-1} between 2.5 and 4.2 V.

Thermal characterization of the ground powders of $LiFePO_4$ was done on a PerkinElmer 7 differential scanning calorimeter (DSC). The measurements were performed in a nitrogen atmosphere between 323 and 673 K, at a heating rate of 10 K min^{-1}. The samples for the DSC investigations were prepared as follows. The coin cells were first galvanostatically charged to 4.3 V at a 0.2 C rate and then potentiostated at 4.3 V for 10 h. The coin cells were dismantled in an argon-filled glove box and the charged cathode was carefully removed. The cathode was then washed with DEC. The excess electrolyte was wiped off and dried. The cathode material was gently scraped from the aluminum current collector, loaded on to an aluminum pan, hermetically sealed, placed in an airtight container, and transferred to the DSC instrument.

3. Results and discussion

3.1. Dynamic light scattering

Before grinding, the average particle sizes of Com-LFP and Lab-LFP powders were 484 and 618 nm, respectively, with two distinct particle-size regions for fresh samples, as shown in Fig. 1(I) and (III). All DLS measurements in this work were based on 50% volume fraction in order to provide a clear comparison of samples in a small range of particle sizes.

After ball-milling of 3, 12, and 18, both Com-LFP and Lab-LFP powders achieved three different particle sizes: 418, 292, 202 nm and 462, 315, 188 nm, respectively, as shown in Fig. 1a–c and d–f. Similarly, both Com-LFP/C and Lab-LFP/C powders also displayed three different particle sizes: 456, 337, 232 nm and 476, 324, 205 nm, respectively, as shown in Fig. 2a–c and d–f. The particle distribution of all separated samples was in one region, which gradually decreased and narrowed as the degree of milling and sieving increased, resulting in a small, homogeneous particle size.

3.2. Morphology

The SEM images obtained for Com-LFP/C and Lab-LFP/C are shown in Fig. 3a–c and d–f, respectively. These carbon composites were prepared by treating their corresponding ground powders of $LiFePO_4$ in Fig. 1 with 50 wt.% malonic acid heating at 873 K for 12 h in Ar/H_2 (vol. 95:5) atmosphere. A similar trend in surface morphology and particle size was observed for Com-LFP/C and Lab-LFP/C in Fig. 3, indicating a gradual decrease in particle size with longer milling times.

Specifically, a slight increase in particle size after carbon coating was detected by DLS measurements. (e.g. 418–456 nm for the 3 h-ball-milled Com-LFP sample to Com-LFP/C composite; 462–476 nm for the 3 h-ball-milled Lab-LFP sample to Lab-LFP/C composite.) Under the above carbon coating condition, no significant and big aggregates were formed.

The particles of the sample ground with shorter milling times were larger and uneven as shown in Fig. 3a and d, but with longer milling times were smaller, uniform and smooth, as shown in Fig. 3c

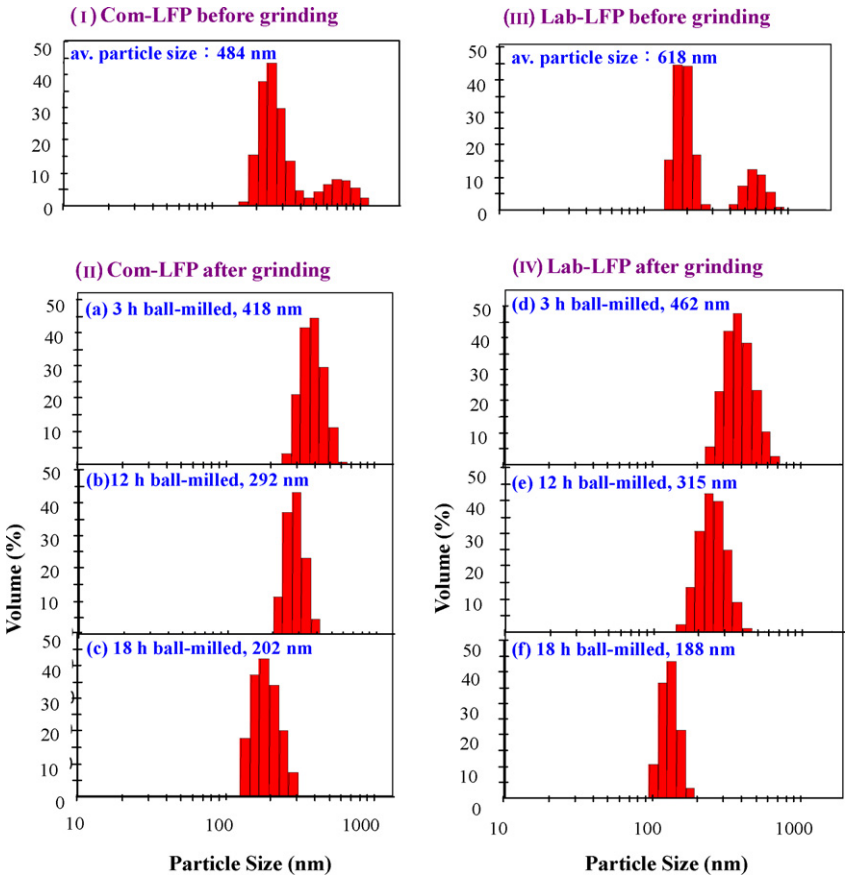

Fig. 1. Particle size distribution of the commercial and in-house bare $LiFePO_4$ samples before and after grinding.

and f. The samples that were reground about 6 times or 18 h had homogeneous particles around 200 nm.

In order to confirm the carbon structure and morphology in detail, we studied these composite materials of different particle sizes further by TEM/SAED/EDS techniques. A 200-mesh copper grid coated with a silicon monoxide film instead of carbon was used to ensure that any carbon detected was from the sample. Our selection of grid prevents any controversy that carbon could have come from the grid, although Cu, Si and O peaks were present as impurities or background in the EDX spectrum. Figs. 4a and 5a,

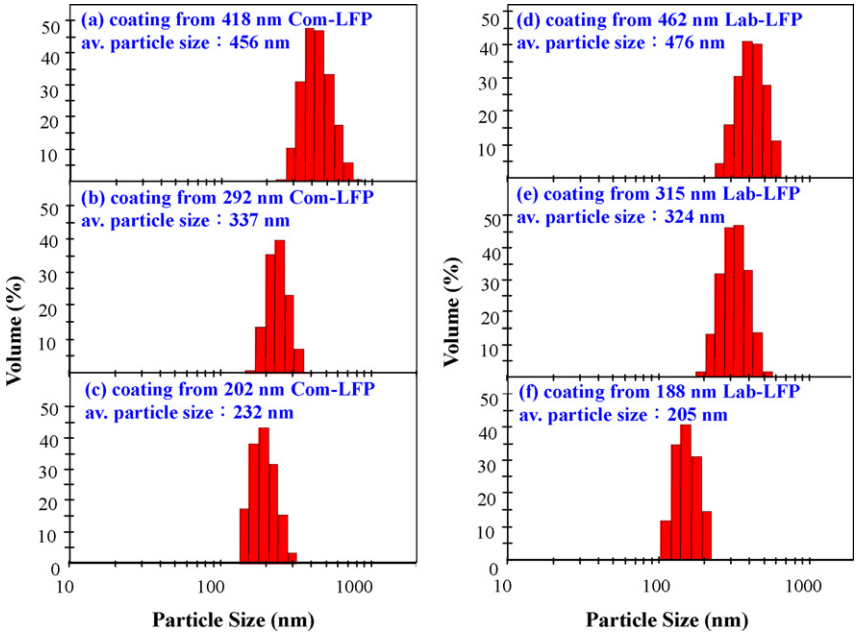

Fig. 2. Particle size distribution of the ground commercial and in-house bare $LiFePO_4$ powders coated with carbon.

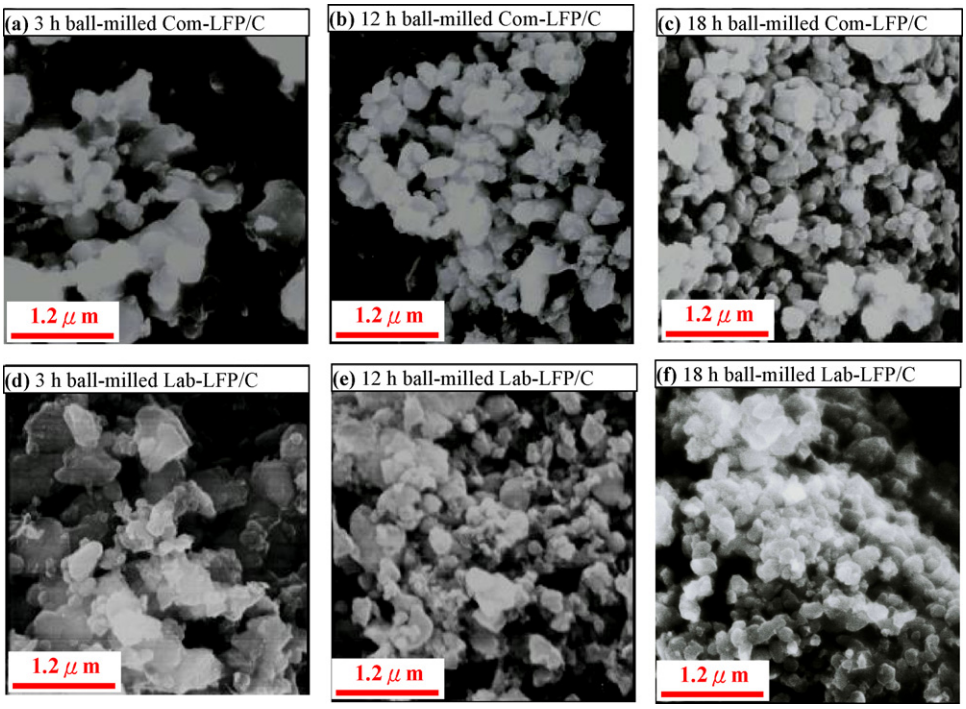

Fig. 3. SEM images of the carbon-coated powders for the commercial and in-house bare samples denoted as Com-LFP/C and Lab-LFP/C, respectively. Com-LFP/C: (a) 3 h ball-milled, (b) 12 h ball-milled, (c) 18 h ball-milled; Lab-LFP/C: (d) 3 h ball-milled, (e) 12 h ball-milled, (f) 18 h ball-milled.

respectively, are the TEM images of the 202 nm Com-LFP/C and 188 nm Lab-LFP/C samples coated with 50 wt.% malonic acid, which indicate that these samples had uniform particle size distribution and an average particle size around 200 nm, which is consistent with what we expected for the ground samples that had long milling times. Figs. 4b and 5b are the magnified images of the outlined areas in Figs. 4a and 5a, which clearly show a uniform coating about 4 nm thick on the particle surface.

The SAED patterns in Figs. 4c,d and 5c,d are used to confirm the $LiFePO_4$/C composite structure in combination with TEM and EDS. Both Figs. 4c and 5c exhibit a bright spot pattern in the core that is typical for crystalline $LiFePO_4$, while Figs. 4d and 5d display a hollow ring pattern typical for amorphous carbon in the outer layer [25]. To clarify their identity, we carried out some EDS analysis. The results are shown in Figs. 4e,f and 5e,f. They definitely confirm that the particle cores are crystalline $LiFePO_4$ and the surface shells are amorphous carbon only.

The average particle size analyzed by DLS, surface area measured by BET, and electronic conductivity determined by the four-point conductivity method for both Com-LFP and Lab-LFP are summarized in Table 1. As particle size decreased, both surface area and electronic conductivity increased. These phenomena have been

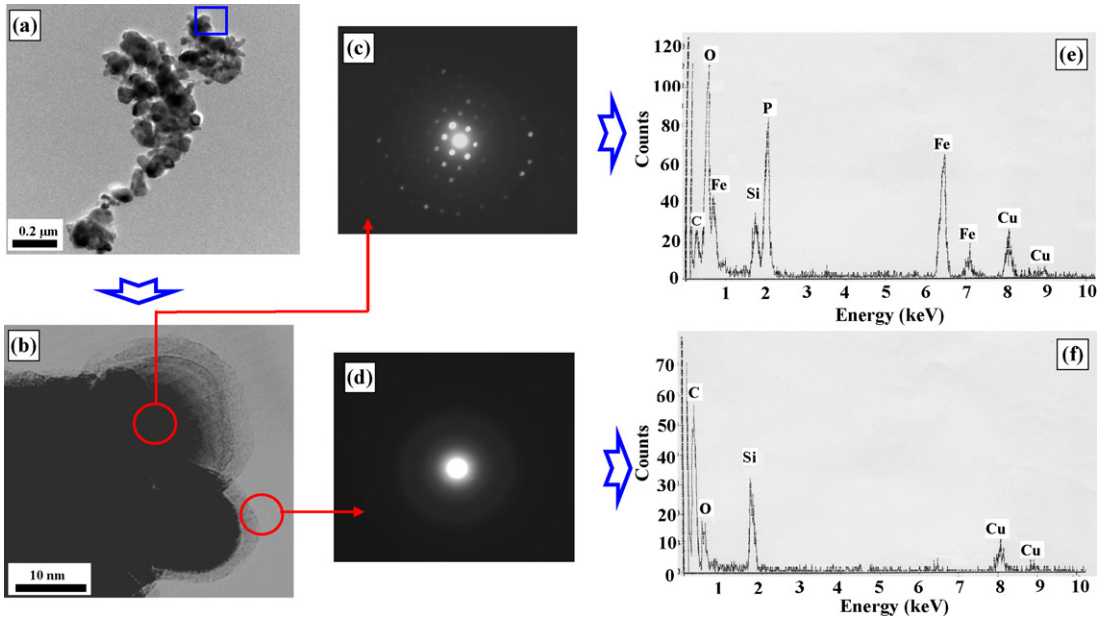

Fig. 4. (a and b) TEM micrographs of 18 h ball-milled commercial $LiFePO_4$/C powders (av. particle size, 232 nm); (c and d) SAED and (e and f) EDS analyses for the particles.

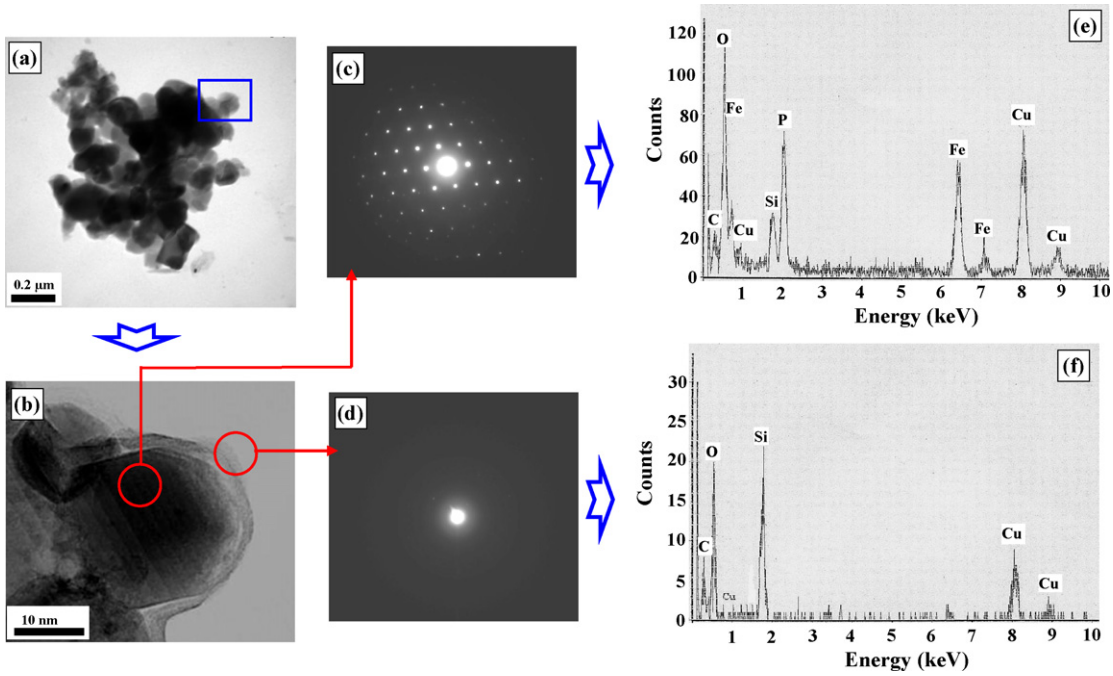

Fig. 5. (a and b) TEM micrographs of 18 h ball-milled in-house $LiFePO_4$/C powders (av. particle size, 205 nm); (c and d) SAED and (e and f) EDS analyses for the particles.

observed by Yamada et al. [5], who reported that improvements in conductivity could be achieved by small and homogeneously sized powders, since smaller-sized particles provide more contact points between particles [26].

Table 2 provides a comparison of our work with selected data on $LiFePO_4$-based electrolytes extracted from Ref. [26]. Our work presents data for more specific particle sizes in the 200–500 nm range that were not studied in Ref. [26], but seem to follow a similar continuous trend in terms of particle size and capacity. Each three samples of Com-LFP/C and Lab-LFP/C had their particles sizes significantly reduced by ball-milling and showed reasonable, consistent battery performance across various average particle sizes. In Table 3, even when there was a large difference in carbon content, the samples that were around the same size displayed similar discharge capacity and electrochemical behavior. In fact, even when the carbon content wt.% had a ratio of Com-LFP/C to Lab-LFP/C of 3:1, this was still the case, which supports Gaberscek's finding that electrode resistance depends primarily on mean particle size and the effect of carbon coating is marginal. However, even though minimization of particle size may be more important to improving cell performance, carbon coating is still required to improve the intrinsic electronic conductivity of $LiFePO_4$. From the XRD data and Scherrer's equation, we calculated the grain size for each of our samples, as listed in Table 3. The ratios of carbon content to surface area were in a narrow range for the samples, which indicates that the surface coating was very similar. As expected, smaller grain sizes resulted in higher surface area and initial discharge capacity, which is consistent with the trend shown in Table 2 for average particle size.

Table 4 compares the initial discharge capacity when different quantities of carbon content are used and compares the quantities used in this work with those cited from references [24,27–29], which ranged from 1.0 to 9.8 wt.%. Our studied carbon wt.% fell within the ranges cited in previous literature and, in fact, even though we used lower carbon content, our capacity numbers were higher than the other studies because the overriding factor that had the most influence on capacity seemed to be particle size.

3.3. X-ray diffraction

Fig. 6 shows the X-ray diffraction (XRD) profiles of 202 nm/232 nm (Com-LFP and Com LFP/C) and 188 nm/205 nm (Lab-LFP and Lab-LFP/C) powders alongside the profiles of amorphous carbon and JCPDS standard $LiFePO_4$. All powders fit a standard $LiFePO_4$ ordered olivine structure indexed by orthorhombic Pnmb. Fig. 6a shows a typical XRD pattern for amorphous carbon that generally displays a noisy background and very poor spectrum quality. All the peaks are broadly shaped, indicating the presence of highly disordered carbon and only the (0 0 2) Bragg peak that results from the stacking of carbon layers appears

Table 1
The powder properties of all commercial and in-house synthesized $LiFePO_4$ and $LiFePO_4$/C samples.

Average particle size (nm)	Surface area ($m^2\,g^{-1}$)		Electronic conductivity ($S\,cm^{-1}$)	
Com-LFP/Com-LFP/C	Com-LFP	Com-LFP/C	Com-LFP	Com-LFP/C
418/456	13	16	1.61×10^{-5}	2.00×10^{-4}
292/337	17	21	5.38×10^{-5}	3.42×10^{-4}
202/232	25	30	8.45×10^{-5}	6.08×10^{-4}
Lab-LFP/Lab-LFP/C	Lab-LFP	Lab-LFP/C	Lab-LFP	Lab-LFP/C
462/476	7	10	1.13×10^{-8}	6.23×10^{-5}
315/324	9	13	1.22×10^{-8}	7.68×10^{-5}
188/205	13	17	1.52×10^{-8}	1.09×10^{-4}

Table 2
A comparison of particle size, carbon content, and initial capacity from this work to selected data on $LiFePO_4$-based electrodes extracted from reference [26].

Particle size range (nm)	Ave. particle size (nm)	Carbon coating/carbon added (wt.%)	Discharge capacity and 1 C ($mAh\,g^{-1}$)	Reference[a]
20–40	30	No/30	163	[26]—[7]
~50	50	Yes/NA	165	[26]—[8]
100–200	140	No/5	158	[26]—[9]
100–300	150	Yes/10	130	[26]—[10]
	205	Yes/50	140	This work (205 nm Lab-LFP/C)
	232	Yes/50	110	This work (232 nm Com-LFP/C)
200–400	300	Yes/5	120	[26]—[11]
	324	Yes/50	102	This work (324 nm Lab-LFP/C)
	337	Yes/50	92	This work (337 nm Com-LFP/C)
	456	Yes/50	84	This work (456 nm Com-LFP/C)
	476	Yes/50	90	This work (476 nm Lab-LFP/C)
~500	500	No/15	115	[26]—[12]
450–550	500	No/10	72	[26]—[13]
315–775	545	No/20	NA	[26]—[14]
600–1000	800	No/5	80	[26]—[15]

[a] The numbers in brackets unlinked denote the reference numbers originally cited in Ref. [26] that are not being included in this work.

significant [30]. In the low two theta (<20°) region, the XRD pattern displays an upturned tail that is an indicator of poor crystallinity [30]. As shown in Fig. 6b and d, the same type of upturn was observed for both 202 nm Com-LFP and 188 Lab-LFP samples, as a result of particles being reduced and damaged from the surface coating during the ball-milling process. After carbon coating, the particle sizes of both composite samples increased slightly as shown in the XRD spectra of Fig. 6c and e. Interestingly, the upturned tail was significantly flatter in these samples, which indicates that the crystallinity of the powder was greatly improved.

3.4. Electrochemical studies

All the ground $LiFePO_4$ samples and their corresponding carbon composites exhibited flat voltage plateaus around 3.32–3.62 V, which was the main characteristic of the two-phase reaction of the lithium extraction and insertion between $LiFePO_4$ and $FePO_4$ [31]. Specific capacity was found to be highly dependent on particle size. Figs. 7 and 8 show the initial charge–discharge curves of Com-LFP and Com-LFP/C. The cells were cycled between 2.8 and 4.3 V at a 0.2 C rate. The discharge capacities for 418, 292 and 202 nm Com-LFP powders were 50, 72 and 91 $mAh\,g^{-1}$, respectively, and 137, 144 and 155 $mAh\,g^{-1}$ for the corresponding carbon composites. These capacity results of commercial ground and carbon coated $LiFePO_4$ powders were compared to the corresponding in-house $LiFePO_4$ powders for evaluation purposes. Under the same cycling conditions, Figs. 9 and 10 display the initial charge–discharge curves of Lab-LFP and Lab-LFP/C. The discharge capacities for 462, 315 and 188 nm-Lab-LFP powders were 15, 21 and 25 $mAh\,g^{-1}$, respectively, and 142, 150 and 157 $mAh\,g^{-1}$ for the corresponding Lab-LFP/C samples.

The effects of particle size on the charge and discharge plateaus, polarization, and initial discharge capacity of $LiFePO_4$ are listed in Table 5. Polarization is related to the difference between the

Table 3
A comparison of grain size and carbon coating between commercial and in-house $LiFePO_4$/C composites.

Average particle size (nm)	Grain size (nm)	Carbon content (wt.%)	Surface area ($m^2\,g^{-1}$)	Carbon content/Surface area (wt.% $g\,m^{-2}$)	Initial discharge capacity at 0.2 C rate ($mAh\,g^{-1}$)
Com-LFP/C					
456	40.22	4.40	16	0.27	139
337	38.37	4.43	21	0.21	147
232	36.71	4.92	30	0.16	155
Lab-LFP/C					
476	42.22	1.08	10	0.10	145
324	37.71	1.33	13	0.10	150
205	35.18	1.62	17	0.09	157

Table 4
A comparison of the initial discharge capacity with the quantity of carbon content from previous literature and this work.

Carbon source	Particle size (nm)	Carbon content (wt.%)	Initial discharge capacity at 0.1 C rate ($mAh\,g^{-1}$)	Reference
60 wt.% malonic acid	416	1.90	155	[24]
3 wt.% PVA (poly vinyl alcohol)	400	1.00	156	[27]
50 wt.% white sucrose	65	6.30	155	[28]
10 wt.% carbon black	870	9.80	136	[29]
Com-LFP/C				
50 wt.% malonic acid	456	4.40	141	This
50 wt.% malonic acid	337	4.43	150	work
50 wt.% malonic acid	232	4.92	161	
Lab-LFP/C				
50 wt.% malonic acid	476	1.08	149	This
50 wt.% malonic acid	324	1.33	153	work
50 wt.% malonic acid	205	1.62	161	

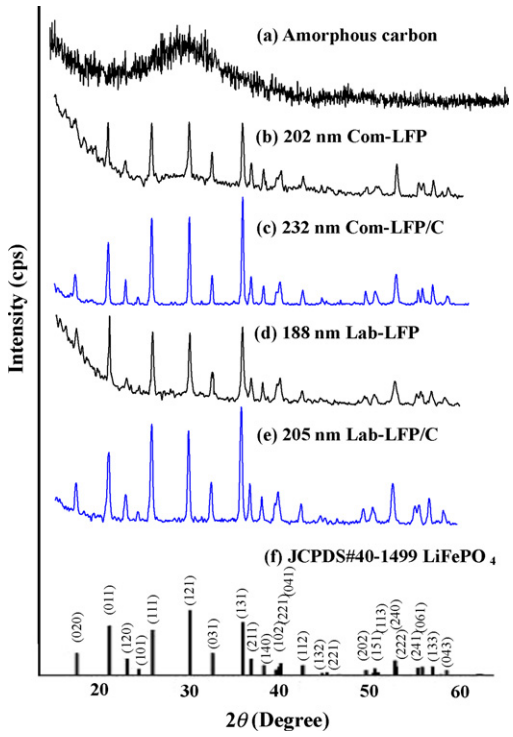

Fig. 6. X-ray diffraction (XRD) patterns: (a) amorphous carbon, (b) 202 nm commercial bare $LiFePO_4$ sample, (c) 232 nm commercial $LiFePO_4$/C composite, (d) 188 nm in-house bare $LiFePO_4$ sample, (e) 205 nm in-house $LiFePO_4$/C composite, (f) JCPDS (#40-1499) $LiFePO_4$.

charge and discharge voltage plateaus [32], which increases with increasing particle size. The sample showing high polarization has a low initial discharge capacity. Both Com-LFP/C and Lab-LFP/C samples with conductive carbon coating exhibited much higher discharge capacity compared to uncoated counterparts. The inferior performance of Com-LFP and Lab-LFP in discharge capacity was attributed to their low electronic conductivity, high polarization and inherently poor kinetics. Before grinding, the discharge capacity of commercial $LiFePO_4$ samples with carbon coating was in a range between 130 and 140 mAh g^{-1}, whereas the in-house pure $LiFePO_4$ sample without carbon coating was 108 mAh g^{-1}.

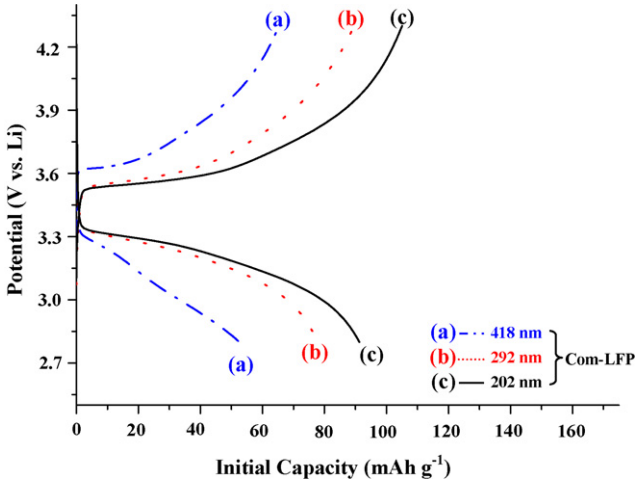

Fig. 7. The initial charge and discharge profiles of commercial bare $LiFePO_4$ samples under different milling times before carbon coating. Average particle sizes: (a) 418 nm, (b) 292 nm, (c) 202 nm; at a 0.2 C rate in the voltage range of 4.3–2.8 V.

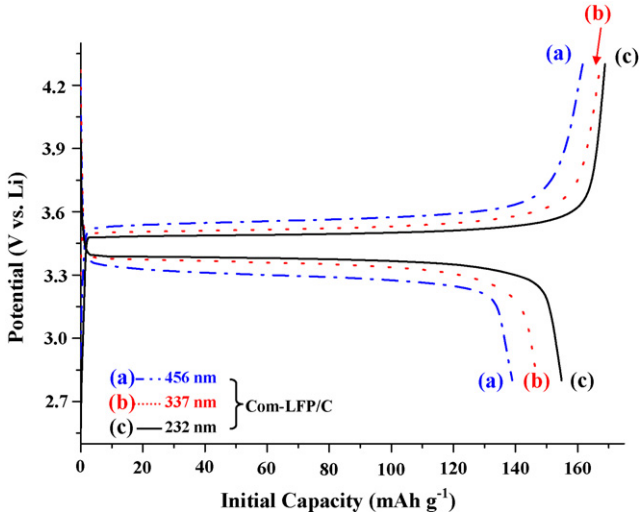

Fig. 8. The initial charge and discharge profiles of commercial bare $LiFePO_4$ samples under different milling times after carbon coating. Average particle sizes: (a) 456 nm, (b) 337 nm, (c) 232 nm; at a 0.2 C rate in the voltage range of 4.3–2.8 V.

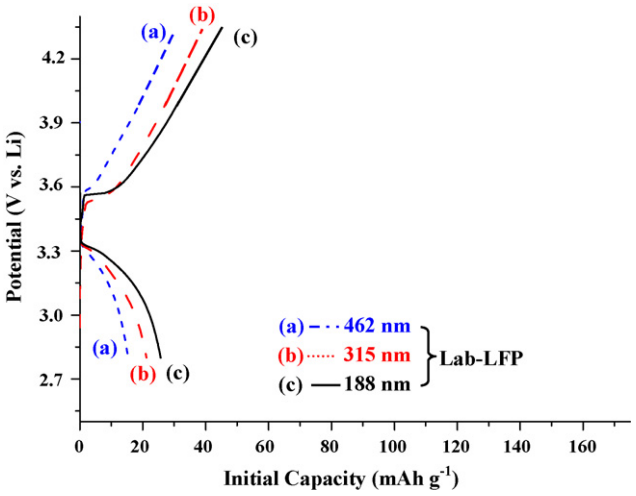

Fig. 9. The initial charge and discharge profiles of in-house bare $LiFePO_4$ samples under different milling times before carbon coating. Average particle sizes: (a) 462 nm, (b) 315 nm, (c) 188 nm; at a 0.2 C rate in the voltage range of 4.3–2.8 V.

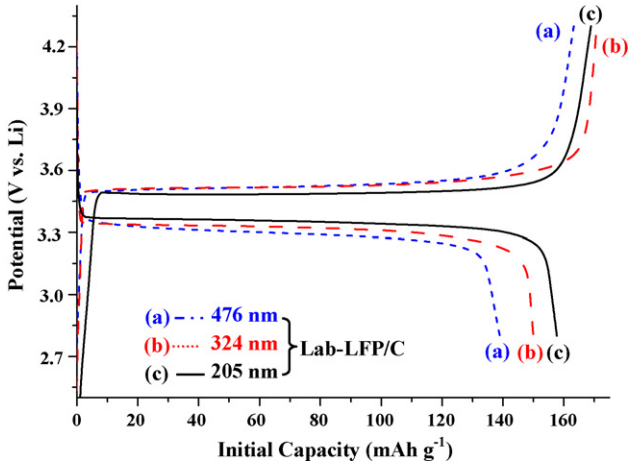

Fig. 10. The initial charge and discharge profiles of in-house bare $LiFePO_4$ samples under different milling times after carbon coating. Average particle sizes: (a) 476 nm, (b) 324 nm, (c) 205 nm; at a 0.2 C rate in the voltage range of 4.3–2.8 V.

Table 5
A comparison of average particle size with the charge and discharge plateaus, polarization, and initial discharge capacity of $LiFePO_4$.

Sample	Average particle size (nm)	Charge voltage plateau (V)	Discharge voltage plateau (V)	ΔV (V)	Initial discharge capacity (mAh g^{-1})
Com-LFP	418	3.62	3.32	0.30	52
	292	3.54	3.34	0.20	72
	202	3.52	3.36	0.16	91
Com-LFP/C	456	3.53	3.35	0.18	139
	337	3.50	3.38	0.12	147
	232	3.49	3.39	0.10	155
Lab-LFP	462	3.58	3.32	0.26	15
	315	3.53	3.34	0.19	21
	188	3.52	3.36	0.16	25
Lab-LFP/C	476	3.53	3.35	0.18	145
	324	3.51	3.37	0.14	150
	205	3.48	3.39	0.09	157

ΔV: the difference between the charge and discharge voltage plateaus.

After grinding, the Com-LFP samples sustained higher initial discharge capacity than Lab-LFP samples, because the former had a carbon coating treatment and some residual carbon remained in the ground powders.

These polarization results for Com-LFP/C and Lab-LFP/C were in accordance with the CV profiles. As illustrated in Figs. 11 and 12, the CV profiles of Com-LFP/C and Lab-LFP/C in the first cycle, respectively, show that the anodic and cathodic peak intensities of the big 456 and 476 nm diameter particles were much lower than those of the small 232 and 205 nm diameter particles. The shape of the peaks are less sharp and more broadened, indicating the kinetic restriction of the lithium diffusion in the larger particle-size samples. The sharp peaks of the small 232 and 205 nm diameter particles show their excellent kinetics [30,33]. An improvement in the kinetics of lithium ion intercalation and deintercalaction could be attributed to the smaller particles that reduced the diffusion length of lithium ions in $LiFePO_4$ [34]. In addition, the voltage difference between the anodic and cathodic peaks is indication of polarization. The more broadened the peak difference, the higher the electrode polarization.

Figs. 13 and 14 show the rate performance of 232 and 456 nm diameter Com-LFP/C particles and 205 and 476 nm diameter Lab-LFP/C particles, respectively. In the case of small Com-LFP/C composites in Fig. 13, the 232 nm diameter particles reached a reversible capacity of 161 mAh g^{-1} at 0.1 C rate and 10 mAh g^{-1} at

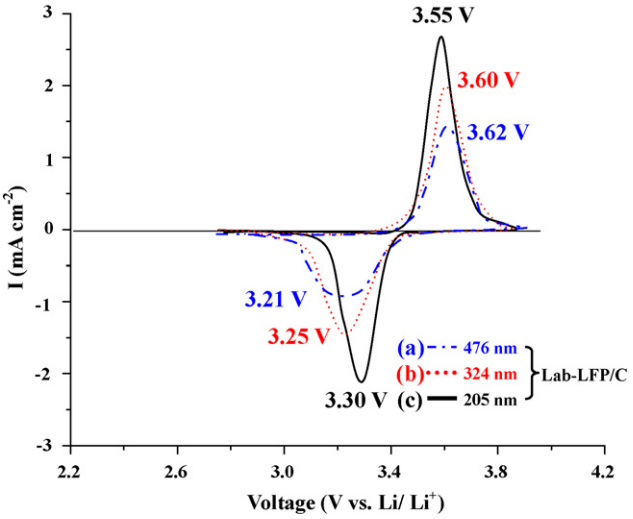

Fig. 12. The CV results of in-house carbon-coated $LiFePO_4$ samples. Average particle sizes: (a) 476 nm; (b) 324 nm; (c) 205 nm. Scanning rate: 0.1 mV s^{-1}. Voltage range: 2.5–4.2 V.

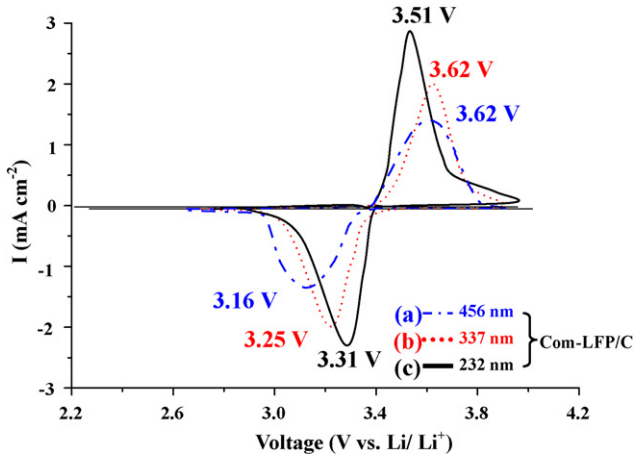

Fig. 11. The CV results of commercial carbon-coated $LiFePO_4$ samples. Average particle sizes: (a) 456 nm; (b) 337 nm; (c) 232 nm. Scanning rate: 0.1 mV s^{-1}. Voltage range: 2.5–4.2 V.

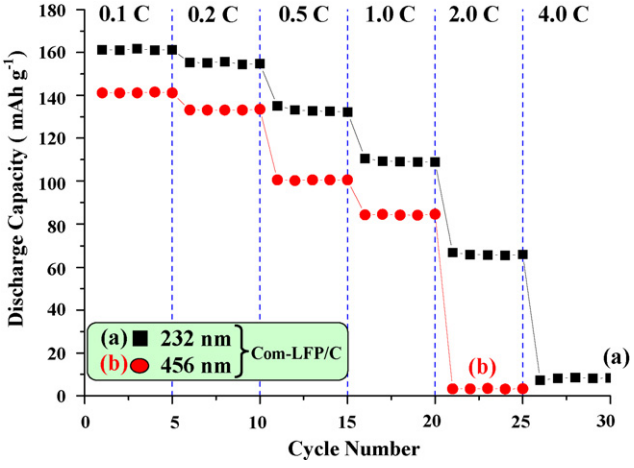

Fig. 13. The rate performance of commercial carbon-coated $LiFePO_4$ samples with small and large particle sizes: (a) 232 nm, (b) 456 nm. The sample was cycled 5 times at each rate and forwarded to the next step.

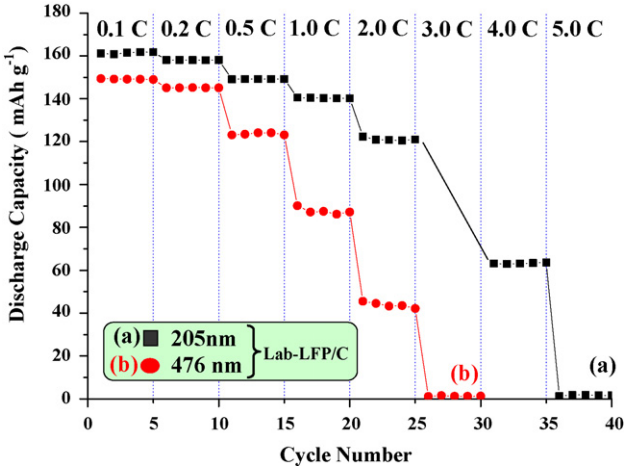

Fig. 14. The rate performance of in-house carbon-coated $LiFePO_4$ samples with small and large particle sizes: (a) 205 nm, (b) 476 nm. The sample was cycled 5 times at each rate and forwarded to the next step.

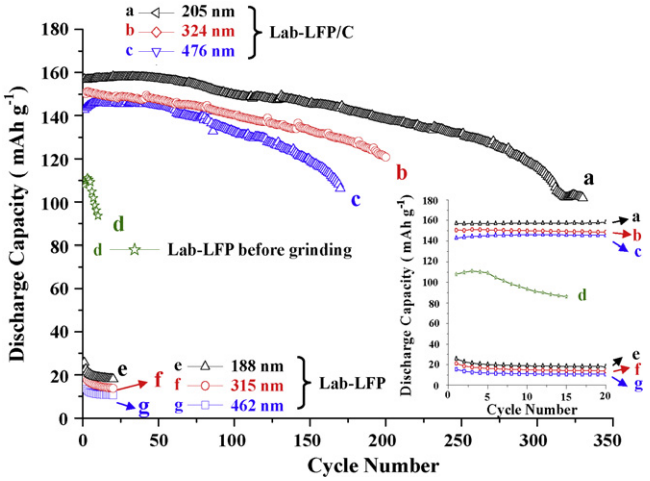

Fig. 16. Cycling performance of in-house ground $LiFePO_4$ samples with three particle sizes after carbon coating: (a) 205 nm, (b) 324 nm, (c) 476 nm; and in-house bare $LiFePO_4$ samples before and after grinding: (d) no grinding, (e) 188 nm, (f) 315 nm, (g) 462 nm; at a 0.2 C rate in the voltage range of 4.3–2.8 V.

4 C rate. However, in the case of small Lab-LFP/C composites in Fig. 14, the 205 nm diameter particles achieved a reversible capacity of 162 mAh g^{-1} at 0.1 C rate and 63 mAh g^{-1} at 4 C rate, and could extend as high as 5 C.

In contrast, the discharge capacity of the big particle size sample deteriorated more dramatically at high current densities compared to the small particle size sample. Similar phenomena were also reported previously [35] and may be due to the intrinsic lithium-ion diffusion limitations of the material. As particle size increased, lithium diffusion became increasingly difficult, which resulted in capacity loss during utilization, especially at higher currents. Furthermore, the smaller the particle size, the easier it is for the electrolyte to penetrate across the whole active material during the charge and discharge process. In this way, lithium ions and electrons are distributed around the entire particle surface, and thus can greatly improve the electrochemical reaction [1,36].

The cycling behavior of different particle sizes of both Com-LFP and Com-LFP/C samples at a 0.2 C rate is plotted in Fig. 15. A similar plot for Lab-LFP and Lab-LFP/C samples is presented in Fig. 16. After ball-milling, both Com-LFP and Lab-LFP powders showed a distinct low discharge capacity, as shown in Fig. 15d–f and Fig. 16d–f, because Lab-LFP did not have a carbon coating and Com-LFP suffered partial oxidation from coating damage that occurred during the ball-milling process. In contrast, the discharge capacities of Com-LFP/C (Fig. 15a–c) and Lab-LFP/C (Fig. 16a–c) were significantly restored after carbon coating treatment. The slight difference in discharge capacity could be attributed to a difference in particle size. It is worth noting that all Com-LFP/C and Lab-LFP/C samples prepared using malonic acid as a carbon source achieved a high capacity near 160 mAh g^{-1} and a very flat capacity curve in the first 20 cycles, as shown in the insets of Figs. 15 and 16, most likely because of uniform particle size distribution and effective carbon coating. The capacity curve remained quite stable after prolonged cycling, possibly due to intimate carbon contact between active material particles. This result is comparable to the one obtained with TEM images. Furthermore, cycle stability decreases as particle size increases, as reflected in the cycle-life results of 420 and 274 cycles achieved by the small 232 and 205 nm diameter Com-LFP/C samples, respectively.

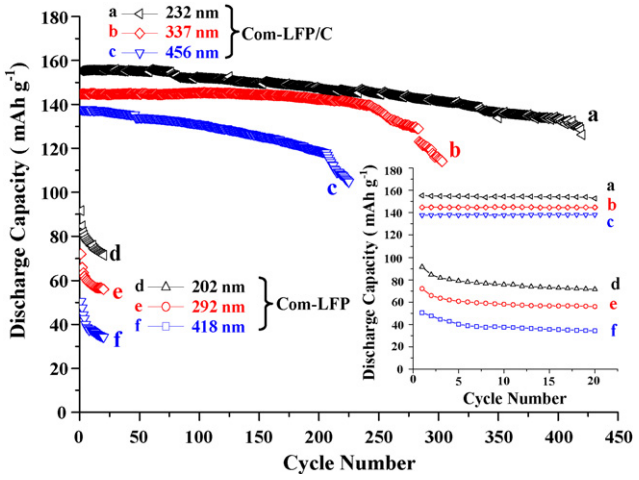

Fig. 15. Cycling performance of commercial carbon-coated and bare $LiFePO_4$ samples denoted as Com-LFP/C and Com-LFP, respectively, with three particle sizes. Com-LFP/C: (a) 232 nm, (b) 337 nm, (c) 456 nm; Com-LFP: (d) 202 nm, (e) 292 nm, (f) 418 nm; at a 0.2 C rate in the voltage range of 4.3–2.8 V.

3.5. DSC

The DSC traces of the overcharged Com-LFP/C and Lab-LFP/C samples with electrolytes are shown in Figs. 17 and 18, when major exothermic heat flow occurred in a wide temperature range of 475–575 K and had a sharp exothermic peak at about 530 K, with total heat evolution of about 94 J g^{-1}. Compared to bare-$LiCoO_2$, all commercial and in-house $LiFePO_4$/C samples appear to have an increase in onset temperature (421–528 K) and a decrease in exothermic enthalpy (164–94 J g^{-1}). The average of exothermic enthalpy for all six samples was 92.5 J g^{-1}.

Interestingly, the DSC profiles of all six particle sizes of $LiFePO_4$/C samples in Figs. 17 and 18, including onset temperature, decomposition temperature and exothermic enthalpy, are almost the same, independent of particle size. This observation in thermal stability was quite similar to that from Jiang and Dahn's work [37], who reported that with the addition of $LiPF_6$ to EC/DEC, self-heating exotherms began at approximately 190 °C for all three $LiFePO_4$ samples, independent of particle size. However, the particle sizes used in Jiang and Dahn's work were 3, 7 or 15 μm, while the particle sizes used in this work were approximately 200, 300, and 400 nm. It is apparent that particle size has negligible effects on the reac-

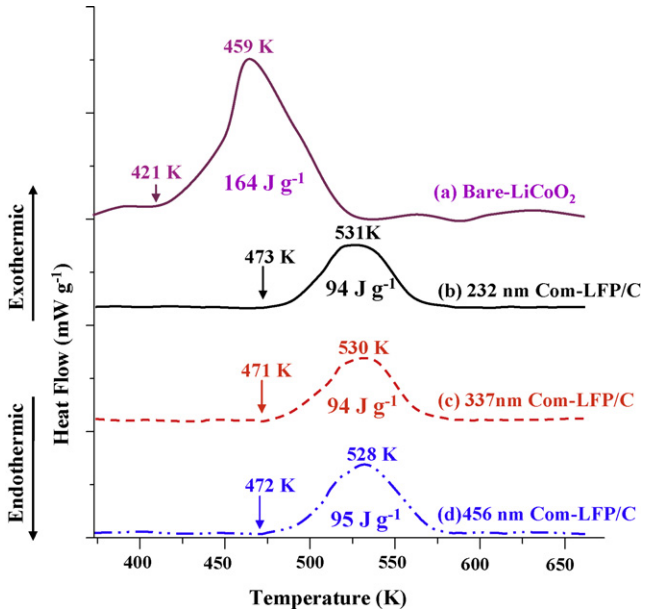

Fig. 17. Differential scanning calorimetry (DSC) traces of (a) bare-$LiCoO_2$ powders and commercial carbon-coated $LiFePO_4$ samples: (b) 232 nm, (c) 337 nm, (d) 456 nm.

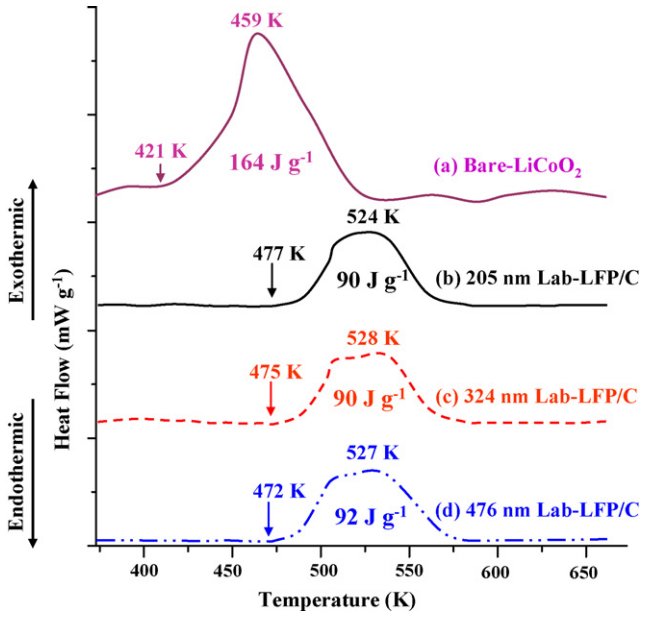

Fig. 18. Differential scanning calorimetry (DSC) traces of (a) bare-$LiCoO_2$ powders and in-house carbon-coated $LiFePO_4$ samples: (b) 205 nm, (c) 324 nm, (d) 476 nm.

tivity between $LiFePO_4$ and the electrolyte. Nevertheless, electrode designers have flexibility to choose particle size for $LiFePO_4$ electrodes, at least from a safety point of view.

4. Conclusions

A simple and low-cost ball-milling method was successfully used to prepare various distinct particle sizes of $LiFePO_4$ cathode materials ranging from 188 to 462 nm under different milling times. The average particle sizes of these ground or carbon-coated cathode materials were measured by DLS technique with a standard deviation of ±10 nm. Three particle sizes of each commercial and in-house prepared $LiFePO_4$ powders, around 200, 300, and 400 nm, were selected and compared for an evaluation and reproducibility study. As particle size decreased, both related surface area and electronic conductivity increased due to more contact points between particles. Furthermore, the smaller particle size $LiFePO_4$ or $LiFePO_4$/C samples showing weak polarization not only provided higher initial discharge capacity, but also more cycles. Both Com-LFP/C and Lab-LFP/C samples treated with malonic acid exhibited much higher discharge capacity compared to uncoated counterparts. It is also worth noting that all small Com-LFP/C and Lab-LFP/C particles achieved 5 C high rate capability and high initial capacity near 160 mAh g^{-1} with a very flat capacity curve in the first 50 cycles due to uniform particle size distribution. Interestingly, we observed that particle size has negligible effect on the reactivity between $LiFePO_4$ and the electrolyte, which will allow us to have a free hand in choosing particle size for $LiFePO_4$ electrode application when considering safety concerns.

Acknowledgement

Financial support for this work was provided by the National Science Council of the Republic of China under contract No. NSC96-2218-E-008-003.

References

[1] A.K. Padhi, K.S. Nanjundaswamy, J.B. Goodenough, J. Electrochem. Soc. 144 (1997) 1188.
[2] F. Sauvage, E. Baudrin, L. Gengembre, J.M. Tarascon, Solid State Ionics 176 (2005) 1869.
[3] D.D. MacNeil, Z. Lu, Z. Chen, J.R. Dahn, J. Power Sources 108 (2002) 8.
[4] A.K. Padhi, K.S. Nanjundaswamy, C. Masquelier, S. Okada, J.B. Goodenough, J. Electrochem. Soc. 144 (1997) 1609.
[5] A. Yamada, S.C. Chung, K. Hinokuma, J. Electrochem. Soc. 148 (2001) A224.
[6] P.P. Prosini, M. Lisi, S. Scaccia, M. Carewska, F. Cardellini, M. Pasquali, J. Electrochem. Soc. 149 (2002) A297.
[7] A.S. Andersson, J.O. Thomas, J. Power Sources 97 (2001) 498.
[8] G. Arnold, J. Garche, R. Hemmer, S. Ströbele, C. Vogler, M.W. Mehrens, J. Power Sources 119 (2003) 247.
[9] P.P. Prosini, M. Carewska, S. Scaccia, P. Wisniewski, S. Passerini, M. Pasquali, J. Electrochem. Soc. 149 (2002) A886.
[10] H. Huang, S.C. Yin, L.F. Nazar, Electrochem. Solid-State Lett. 4 (2001) A170.
[11] H. Gabrisch, J.D. Wilcox, M.M. Doeff, Electrochem. Solid-State Lett. 9 (2006) A360.
[12] H.T. Chung, S.K. Jang, H.W. Ryu, K.B. Shim, Solid State Commun. 131 (2004) 549.
[13] P.S. Herle, B. Ellis, N. Coombs, L.F. Nazar, Nat. Mater. 3 (2004) 147.
[14] S.Y. Chung, J.T. Bloking, Y.M. Chiang, Nat. Mater. 1 (2002) 123.
[15] H. Xie, Z. Zhou, Electrochim. Acta 51 (2006) 2063.
[16] J.F. Ni, H.H. Zhou, J.T. Chen, X.X. Zhang, Mater. Lett. 59 (2005) 2361.
[17] S.Y. Chung, Y.M. Chiang, Electrochem. Solid-State Lett. 6 (2003) A278.
[18] H. Tsunekawa, S. Tanimoto, R. Marubayashi, M. Fujita, K. Kifune, M. Sano, J. Electrochem. Soc. 149 (2002) A1326.
[19] M.M. Doeff, Y. Hu, F. McLarnon, R. Kostecki, Electrochem. Solid-State Lett. 6 (2003) A207.
[20] S. Franger, F.L. Cras, C. Bourbon, H. Rouault, J. Power Sources 119 (2003) 252.
[21] G. Meligrana, C. Gerbaldi, A. Tuel, S. Bodoardo, N. Penazzi, J. Power Sources 160 (2006) 516.
[22] S. Yang, P.Y. Zavalij, M.S. Whittingham, Electrochem. Commun. 3 (2001) 505.
[23] Y. Xia, M. Yoshio, H. Noguchi, Electrochim. Acta 52 (2006) 240.
[24] G.T.K. Fey, T.L. Lu, F.Y. Wu, W.H. Li, J. Solid State Electrochem. 12 (2008) 825.
[25] G.T.K. Fey, T.L. Lu, J. Power Sources 178 (2008) 807.
[26] M. Gaberscek, R. Dominko, J. Jamnik, Electrochem. Commun. 9 (2007) 2778.
[27] N.J. Yun, H.W. Ha, K.H. Jeong, H.Y. Park, K. Kim, J. Power Sources 160 (2006) 1361.
[28] H. Liu, J. Xie, K. Wang, J. Alloys Compd. 459 (2007) 521.
[29] S.H. Ju, Y.C. Kang, Mater. Chem. Phys. 107 (2008) 328.
[30] G.T.K. Fey, D.C. Lee, Y.Y. Lin, T.P. Kumar, Synthetic Metals 139 (2003) 71.
[31] M. Takahashi, S. Tobishima, K. Takei, Y. Sakurai, J. Power Sources 97 (2001) 508.
[32] H. Chen, S.C. Han, W.Z. Yu, H.Z. Bo, C.L. Fan, Z.Y. Xu, Bull. Mater. Sci. 29 (2006) 689.
[33] S.S. Zhang, J.L. Allen, K. Xu, T.R. Jow, J. Power Sources 147 (2005) 234.
[34] L. Wang, Y. Huang, R. Jiang, D. Jia, J. Electrochem. Soc. 154 (2007) A1015.
[35] T. Drezen, N.H. Kwon, P. Bowen, I. Teerlinck, M. Isono, I. Exnar, J. Power Sources 174 (2007) 949.
[36] Z. Xu, L. Xu, Q. Lai, X. Ji, Mater. Chem. Phys. 105 (2007) 80.
[37] J. Jiang, J.R. Dahn, Electrochem. Commun. 6 (2004) 724.